Geomechanics and Engineering, *Vol. 40, No. 5 (2025) 379-393*
https://doi.org/10.12989/gae.2025.40.5.379

Assessing the influence of sequential basement excavation and tunneling on a pile in stiff clay: A 3D coupled consolidation approach

Naeem Mangi[1,2], Qian Su*[1,3], Zongyu Zhang[1], Yanfei Pei[1,4] and Aibo Luo[1]

[1]*School of Civil Engineering, Southwest Jiaotong University, Chengdu 610031, China*
[2]*Department of Civil Engineering, Quaid-e-Awam University of Engineering, Science & Technology, Sindh, Pakistan*
[3]*Sichuan College of Architectural Technology, Deyang, 618000, China*
[4]*Key Laboratory of High-Speed Railway Engineering of Ministry of Education, Southwest Jiaotong University, Chengdu, Sichuan 610031, China*

(*Received November 21, 2024, Revised February 6, 2025, Accepted February 19, 2025*)

Abstract. Urban development often necessitates underground construction activities such as basement excavations and tunneling, in close proximity to existing pile foundations supporting high-rise structures. This study investigates the combined effects of basement excavation followed by tunneling on single pile foundation in stiff clay using three-dimensional coupled consolidation numerical modelling. To ensure realistic soil behaviour, an advanced hypoplastic constitutive model for clay was employed, incorporating small-strain stiffness, and stress dependent dilatancy of soil. This research focuses on the response of single piles subjected to sequential basement excavation and tunnelling activities. A parametric study was conducted, analyzing three different basement excavation depths and three tunnel positions relative to the pile. These combinations include scenarios where the formation levels and tunnel depths are near the pile shaft (SeSt case), near the pile toe (TeTt case), and below the pile toe (BeBt case). In each scenario, the tunnel excavation was simulated after the basement excavation. The results reveal that tunnelling following basement excavation induces significant pile settlement and alters axial load redistribution along the pile, primarily due to stress release and degradation of soil stiffness. Among the three scenarios, the BeBt case exhibited the maximum pile settlement of 63.1 mm, equivalent to 7.9% of the pile diameter. The TeTt case recorded the highest induced bending moment of 328 kNm, accounting for 43.7% of the bending capacity of the pile. Additionally, the BeBt scenario resulted in the greatest deflection at the pile toe due to basement excavation. These findings provide critical insights for practitioners in assessing pile performance during sequential excavation and tunneling activities.

Keywords: parametric study; pile; sequential excavation and tunnelling; settlement

1. Introduction

Urban development has increased underground construction activities, such as tunnelling and deep excavations, creating challenges for nearby pile foundations that support high-rise buildings. Pile foundations transfer structural loads into the ground; while tunnelling and excavation relieve soil stress, leading to ground movements. In cities with limited surface space, underground transit systems are increasingly used to ease congestion, but their construction near existing structures poses risks to structural integrity (Ding *et al.* 2017, Jeon and Lee 2023, Liu *et al.* 2023, Shi *et al.* 2019, 2023). Deep excavations near existing buildings can cause soil deformation, affecting pile foundations' safety and serviceability, as documented by multiple studies (Cui *et al.* 2021, Finno *et al.* 1991, Goh *et al.* 2003, Poulos and Chen 1997). This makes understanding soil-pile interaction during construction crucial for urban infrastructure**.** The interaction between pile foundations, basement excavation, and tunnelling in stiff clay presents significant geotechnical challenges. Numerous studies have explored this interaction through field monitoring, centrifuge tests, analytical solutions, and numerical modelling (Boonyarak and Ng 2014, Chiang and Lee 2007, Fang *et al.* 2023, Jacobz 2003, Jeon *et al.* 2024, Kim *et al.* 2024, Loganathan *et al*. 2000, Mroueh and Shahrour 2002a, Ng *et al.* 2013). These studies consistently show that tunnelling adjacent to pile foundations induces pile settlement, additional axial loads, and bending moments, which negatively affect foundation stability. The magnitude of these effects depends on factors such as the distance between the tunnel and the pile and the depth of excavation.

Research on the impact of basement excavation on pile foundations has highlighted the importance of excavation depth and soil characteristics. Extensive field tests (Finno *et al.* 1991, Goh *et al*. 2003), centrifuge tests (Leung *et al.* 2000), and numerical modelling (Poulos and Chen 1996) have shown that deeper excavations lead to greater pile displacement, especially in cases where piles are located near the excavation boundary. Studies by (Shaaban *et al.* 2023) and (Zheng *et al.* 2012) also suggest that excavation depth influences the mobilization of shaft resistance, causing additional pile settlement and lateral deflection. Tunnelling near piles introduces vertical settlement and lateral displacement, especially when the tunnel is located close to the pile. (Lim *et al.* 2023) found that tunnelling in

*Corresponding author, Professor
E-mail: tmsq@home.swjtu.edu.cn

ISSN: 2005-307X (Print), 2092-6219 (Online)

stiff clay releases stress, leading to the redistribution of forces on adjacent piles. The tunnel's proximity and construction sequence are crucial in determining the extent of these effects. (Bezuijen and van der Schrier 1994) and (Loganathan *et al.* 2000) studied tunnelling impacts, revealing that tunnels drilled too close to piles can cause significant settlement. (Loganathan *et al.* 2000) and (Jacobz 2003) found that tunnelling in soil increases the bending of piles and the forces along their length. Similarly, (Mroueh and Shahrour 2003) used three-dimensional models to show that piles further from the tunnel face experience less force and bending. (Pang *et al.* 2005) documented that piles near tunnel excavations experience considerable settlement and lateral forces due to stress relief. (Ng *et al.* 2013) confirmed through three-dimensional centrifuge modelling that tunnelling-induced settlement and deformation are exacerbated in stiff soil compared to softer soils. Research on combined tunneling and excavation effects has been relatively limited, especially concerning their impact on piles in stiff clay. (Korff *et al.* 2016) studied the influence of multi-prop basement excavations on pile behavior in stiff soils, noting that while proper support systems mitigate some adverse effects, they do not eliminate stress redistribution entirely. Tunnelling near piles exerts vertical and lateral forces, while excavation induces lateral movement in the opposite direction, creating a complex scenario for pile behavior. Recent studies (Shi *et al*. 2022) have explored the combined effects of sequential and simultaneous basement excavations, finding that simultaneous excavation significantly reduces the maximum bending moment in piles. Centrifuge and numerical modeling have provided deeper insights into these combined effects, showing that pile settlements and tilting increase with excavation depth. In a 2022 study, (Shi *et al*. 2022) and colleagues focused on the effects of construction sequences for double basement excavations on nearby floating piles in dry sand, an area previously underexplored with most studies concentrating on single basement excavations and end-bearing piles. Using centrifuge tests and numerical analyses, the researchers discovered that sequential excavations—multi-propped followed by cantilever—result in different impacts: 0.42% d_p pile settlement for multi-propped and 0.72% d_p for cantilever, attributed to changes in soil shear modulus and support system stiffness. Furthermore, while the construction sequence of double basements had limited effects on pile head settlement, simultaneous excavation significantly reduced the maximum bending moment to just 18.9% compared to sequential excavation. The study underscores the advantage of simultaneous over sequential basement construction for maintaining the safety and serviceability of existing pile foundations. Experimental work has also focused on stress release and horizontal soil movements around piles due to tunneling and excavation. Research by (Ong *et al.* 2006) and (Goh *et al*. 2003) emphasized the significant impact of soil-structure interactions on lateral pile deflection and bending moments.

The use of advanced numerical modelling, such as ABAQUS simulations, has emerged as a critical tool for investigating these complex interactions. (Lim *et al.* 2023, Soomro *et al*. 2021, 2023, Xu *et al*. 2024) and others have shown that numerical models can accurately predict pile behavior, settlement, and bending moments in soil. (Cheng *et al.* 2007, Soomro *et al.* 2022, 2023, Xu *et al.* 2025) utilized finite element analysis to model pile response to tunnel advancement, while (Shi *et al.* 2019) applied similar techniques to assess the interaction between piles and deep basement excavation in stiff clay. Both studies demonstrated that accurate prediction of pile behavior requires careful consideration of soil consolidation, stress redistribution, and construction sequence. Advanced constitutive models, such as hypoplastic models, have further improved numerical simulations' accuracy. According to (Herle and Gudehus 1999), hypoplastic models can capture the non-linear behavior of stiff clays, including small-strain stiffness and stress path dependency. These models have been successfully applied in studies (Kolymbas 1991) and (Mašín 2005) to simulate pile response under various tunnelling and excavation scenarios.

Despite the advancements in understanding pile response to individual geotechnical activities, the combined effects of basement excavation and tunneling on piles, particularly in stiff clay, remain underexplored. Existing studies have primarily focused on either tunnelling or excavation, but not in combination. Furthermore, most research has been conducted in soft soil, with limited attention given to stiff clays. This study aims to fill this gap by investigating the combined effects of excavation and tunneling on single piles in stiff clay using three-dimensional coupled consolidation numerical modelling. The findings from this research will provide new insights into pile behavior under complex loading conditions, informing better design practices for foundation systems in urban environments.

2. Three-dimensional coupled consolidation analysis

To gain new insights into the single pile response subjected to combined basement excavation on one side and tunnelling on the other side of the pile in stiff clay, three-dimensional coupled consolidation numerical modelling is carried out in this study.

The elevation views of the three different cases, SeSt, TeTt, and BeBt, are illustrated in Fig. 1 as (a), (b), and (c), respectively. In each case, the sequence involves initial excavation on one side of the single pile, followed by tunnelling on the other side. The dimensions of the soil model are uniform at 70 m x 70 m x 70 m, providing a consistent basis for comparison. Moreover, the specifications regarding the tunnel diameter (6 m), pile length (18 m), and pile diameter (0.8 m) remain constant across all cases. Additionally, the clear distance between the excavation and the pile measures 3.2 m, while the distance between the tunnelling and the pile is 2.6 m. The excavation width and length are 20 m x 20 m in all cases, but the final excavation depths (H_e) vary at 18 m, 27 m, and 36 m in SeSt, TeTt, and BeBt cases, respectively. Similarly, the depth of the diaphragm wall (DW) is 18 m, 27 m, and 36 m, respectively, in all cases. However, the thickness of DW

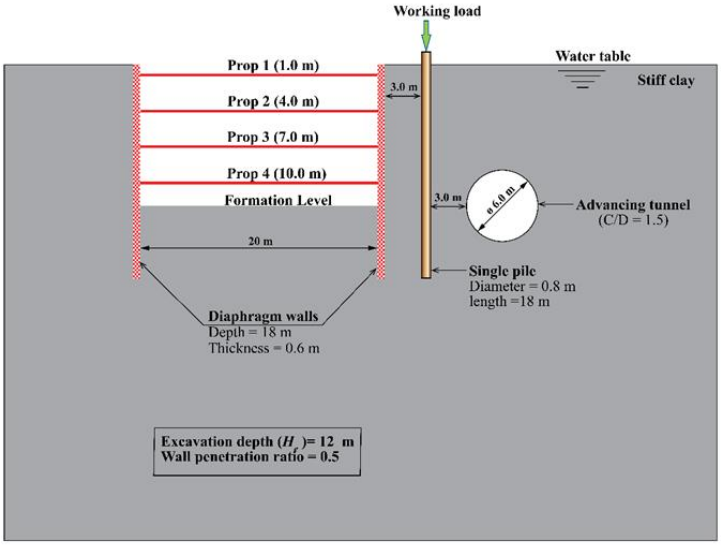

(a)

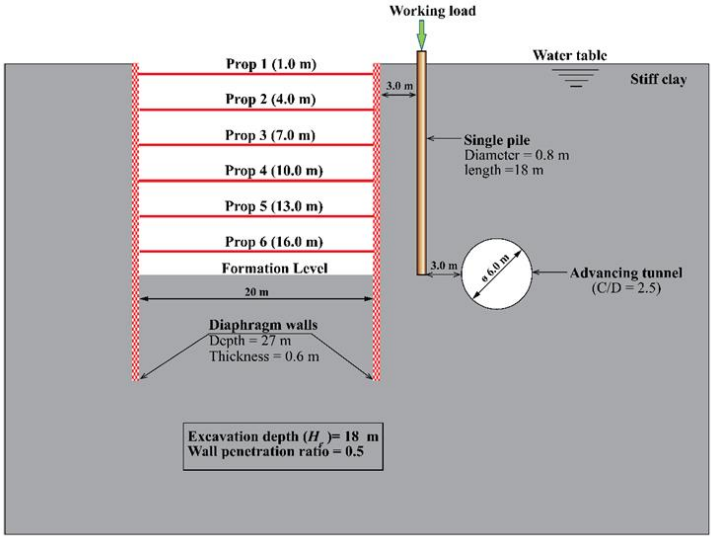

(b)

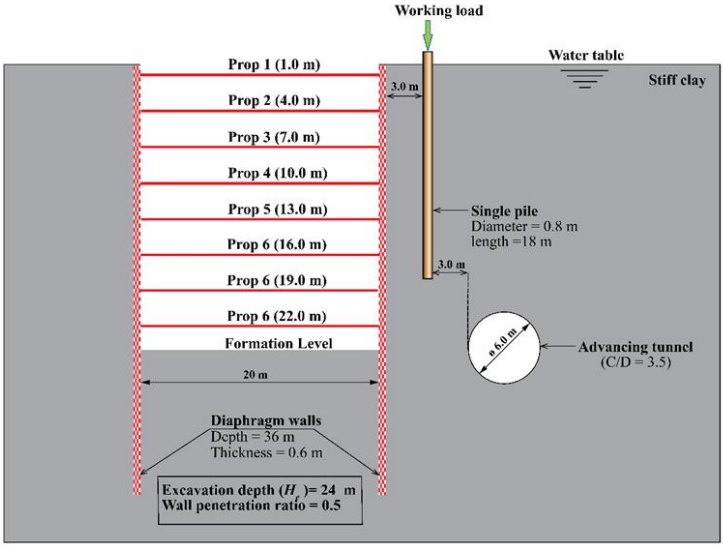

(c)

Fig. 1 Elevation view of numerical simulations of cases (a) SeSt, (b) TeTt and (c) BeBt

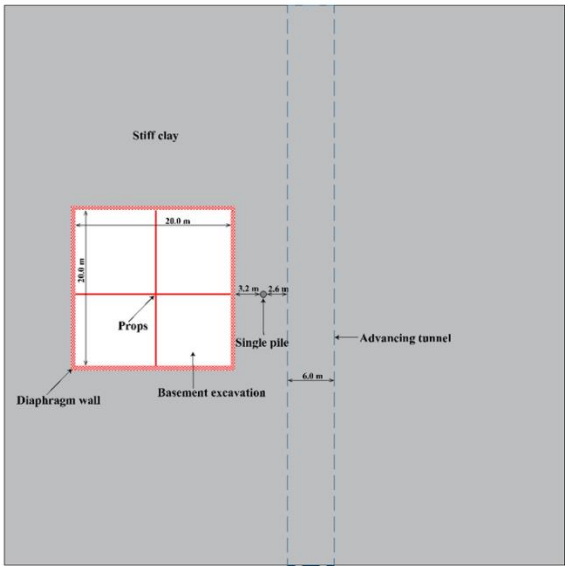

Fig. 2 Numerical simulation Plan view of a typical case of TeTt

Table 1 Summary of numerical analyses

Case ID	H_e/L_p	C/D
SeSt	0.67	1.5
TeTt	1.00	2.5
BeBt	1.33	3.5

remains the same across all cases. The diaphragm walls have a penetration depth ratio (H_p/H_e) of 0.5, which is typical in engineering practice (Hsiung 2009, Ng *et al.* 2013, Shi *et al.* 2022). Different levels of props are mutually perpendicular to each other to support the DWs with a vertical spacing of 3 m. The first level of props is installed 1.0 m below the ground surface. The props (I-section) are modeled as soft with an axial rigidity of $81\times10^{\wedge3}$ kNm (Shi *et al.* 2022). In addition, the working load of 1.08 MN (or 1080 kN) was determined from the load-settlement curve obtained through a numerical pile load test, applying the failure criterion equation proposed by (Ng et al., 2001).

In the SeSt case (Fig. 1(a)), the illustration focuses on excavation and tunnelling near the pile shaft, revealing the specific arrangement and dimensions related to this configuration. For the TeTt case (Fig. 1(b)), the emphasis is on carrying out excavation and tunnelling next to the pile toe. Finally, the BeBt case (Fig. 1(c)) shows the specifics of excavation and tunnelling activities below the pile, highlighting the distinct parameters relevant to this arrangement. The numerical simulation Plan view and the summary of numerical analyses are shown in Fig. 2 and Table 1, respectively.

2.1 Finite element mesh and boundary conditions

Fig. 3 illustrates a three-dimensional finite element mesh of case TeTt. The dimensions of the model are uniformly set at 70 m x 70 m x 70 m, ensuring adequate size to minimize boundary effects on the simulation results, thereby providing accurate and reliable data for engineering analysis.

The mesh employs eight-noded hexahedral brick elements to accurately model the soil, pile, and diaphragm wall, allowing for a detailed representation of the mechanical interactions between them. Four-noded shell elements are utilized to model the tunnel lining, enhancing the simulation's precision regarding the structural behavior during tunnelling operations while two-noded truss elements are adopted to model the props. Boundary conditions include roller supports on the vertical faces and pin supports at the base, effectively restraining movements normal to these boundaries and in all directions at the base.

This setup simulates a realistic underground environment by limiting the influence of the model edges on the simulation results. Hydrostatic conditions are carefully defined, with the water table at ground level and an initial hydrostatic distribution of pore water pressure. Free drainage is permitted at the top of the mesh boundary, while the tunnel lining is assumed to be impervious, influencing the interaction between groundwater and the structural elements. The soil-pile interface is modeled with zero thickness, using duplicate nodes to precisely capture the frictional interactions based on the Coulomb friction law, crucial for analyzing the pile behavior under the applied loads from nearby structural activities. To accurately represent the interaction, appropriate parameters governing both tangential and normal behaviors have been selected for the contact between piles and soil. The Coulomb Friction model has been implemented to define the frictional contact properties, thereby facilitating the simulation of tangential behavior. The interface is modelled by the Coulomb friction law, in which the interface friction coefficient (μ) and limiting displacement (γ_{lim}) are required as input parameters. A limiting shear displacement of 5 mm is assumed to achieve full mobilization of the interface friction equal to $\mu\times$p', where p' is the normal effective stress between two contact surfaces, and a typical value of μ for a bored pile of 0.35 is used in all analyses (Soomro *et al.* 2023). In this study, the displacement-controlled model

Table 2 Kaolin Clay Parameters

Description	Parameter
Effective angle of shearing resistance at critical state, ϕ'	22°
Parameter controlling the slope of the isotropic normal compression line in the ln(1+e) versus ln p plane, λ^*	0.11
Parameter controlling the slope of the isotropic normal compression line in the ln(1+e) versus ln p plane, κ^*	0.026
Parameter controlling the position of the isotropic normal compression line in the ln(1+e)-ln p plane, N	1.36
Parameter controlling the shear stiffness at medium- to large-strain levels, r	0.65
Parameter controlling initial shear modulus upon 180° strain path reversal, m_R	14
Parameter controlling initial shear modulus upon 90° strain path reversal, m_T	11
Size of elastic range, R	1 x 10^{-5}
Parameter controlling the rate of degradation of stiffness with strain, β_r	0.1
Parameter controlling degradation rate of stiffness with strain, χ	0.7
Initial void ratio, e	1.05
Dry density (kg/m³)	1136
Coefficient of permeability, k (m/s)	1 x 10^{-6}

(DCM) was utilized, following the approach proposed by Cheng *et al.* (2007). Prior to the tunneling process, the volume loss was predetermined by defining the dimensions of the gap between the tunnel lining and the excavated soil.

The simulation of the excavation process adjacent to one side of the pile is achieved through the

deactivation of soil elements within the specified excavation zone. Concurrently, the truss elements that represent the supporting props are activated to maintain structural integrity. On the opposite side of the pile, the simulation of tunnelling progresses by similarly deactivating soil elements within the tunnel segment while activating the shell elements that represent the tunnel lining, ensuring the continuity and stability of the tunnel structure. This approach mimics the closed face shield tunnelling technique, with a predefined 2% volume loss set to simulate the effects of soil excavation on the surrounding structures based on empirical data from previous studies on tunnelling in similar geological conditions. The simulated tunnel advancement showcases closed face shield tunnelling effects, adopting a 2% volume loss based on reports by (Abrams 2007, Mair 1997, Shirlaw *et al.* 2003) that noted typical losses ranging from 1% to 4% in various soils.

2.2 Constitutive model and model parameters used in finite element analyses

In Constitutive models and their parameters play a pivotal role in accurately capturing the complex ground deformation induced by unloading, especially considering the significant increase in soil stiffness upon stress path reversal. In this study, an advanced hypoplastic clay model developed by (Mašín 2005), which integrates the intergranular strain concept by (Niemunis and Herle 1997), was employed. This model adeptly captures the non-linear, path-dependent soil stiffness at small strains and has been implemented in the commercial finite element software package Abaqus through a user-defined subroutine.

The fundamental hypoplastic model, initially tailored to describe the non-linear behavior of granular materials under monotonic loading at medium-to-large strain levels (David Mašín and Herle 2005), facilitates the modelling of varying stiffness during loading, unloading, softening, hardening, and volume changes during shearing processes, such as dilation and compression. The model's current stiffness not only depends on the stress path but also on the recent stress history, employing a single non-linear tensorial equation to yield the stress state $\dot{T}$ as a function of the stretching rate D. The general stress-strain relationship is expressed as

$$\dot{T} = f_s L : D + f_s f_d N \|D\| \quad (1)$$

where L and N represent fourth and second-order constitutive tensors, respectively, and f_s and f_d are scalar factors reflecting the influences of barotropy and pyknotropy. This hypoplastic model, enhanced with the intergranular strain concept, includes additional parameters to account for strain dependency and path dependency at small strains, significantly refining the model's predictive accuracy. These parameters, namely R, β_r, χ, m_T and m_R regulate the elastic range's size, stiffness degradation rate, and initial shear modulus upon strain path reversal.

In this study, kaolin clay was selected as the soil model due to its well-documented physical properties and geotechnical characteristics, which have been extensively explored through microstructure characterization, seepage, compression, and shear tests (Al Tabbaa 1987, Benz 2007, Hong *et al.* 2020, Hong *et al.* 2019). Its consistent use as a standard material in simulating soil-pile interaction problems further substantiates its suitability for model tests. The parameters for the hypoplastic clay model, specifically designed for kaolin, were derived from these comprehensive

Table 3 Concrete parameters adopted in finite element analysis

Description	Parameter
Young's Modulus, E	35 GPa
Poisson's ratio, ν	0.3
Density, ρ	2400 kg/m^3

studies (Hong *et al.* 2017). The parameters for the hypoplastic clay model adopted in this study are based on those established in previous research by (Soomro *et al.* 2017). These parameters were rigorously calibrated and validated by the researchers against both the literature and experimental data, including results from tests of cyclic behavior piles in centrifuges, confirming the model's capability to accurately replicate soil behavior under stress path reversals. Notably, the hypoplastic model integrates the intergranular strain concept, enhancing its ability to simulate dynamic soil responses accurately. Out of the ten critical parameters for kaolin clay, four (i.e., N, λ^*, κ^* and φ_c) are well-established in the literature. Based on these foundational parameters, the remaining six parameters governing soil stiffness at medium to large strain levels (r) and small strain levels (i.e., R, β_r, χ, m_T and m_R) were fine-tuned against existing kaolin clay data. These calibrations included comparisons with historical stress-strain relationships provided by (Parry and Nadarajah 1974) and stiffness degradation curves from (Benz 2007). Further validation of these parameters was achieved through comparisons with centrifuge test outcomes reported by (Loganathan *et al.* 2000). Furthermore, the study acknowledges the behavior of overconsolidated clays, which exhibit a pre-consolidation pressure exceeding the current overburden pressure due to unloading or aging effects. As noted by Sivakumar and (Sivakumar *et al.* 2009), the coefficient of lateral earth pressure at rest, K_0, is influenced by the overconsolidation ratio (OCR) and its variation with depth, based on the equation by (Mayne and Kulhawy 1982) which correlates K_0 with OCR.

All model parameters for stiff clay are summarized in Table 2. Additionally, the structural elements such as concrete piles and tunnel linings within the model are assumed to be linear elastic, characterized by Young's modulus of 35 GPa, Poisson's ratio of 0.25, and the unit weight of concrete was set at 24 kN/m³ (see Table 3). This comprehensive modelling approach, incorporating both soil and structural parameters, provides a robust framework for analyzing complex geotechnical interactions under varied loading conditions.

2.3 Numerical modelling procedure

The numerical simulations were conducted following a detailed step-by-step procedure:

First, the finite element model was established with initial boundary and static stress conditions using an at-rest earth pressure coefficient (K_0) of 0.5. The brick elements representing the single pile were then activated as wished-in-place. Next, the working load, determined from the numerical pile load test results, was applied, and excess pore pressure generated from this load was allowed to dissipate completely. The brick elements for the diaphragm wall (DW) were activated for each case, and the staged multi-propped excavation on one side of the pile was simulated, with props installed at specified depths after reaching 3 m. Once excavation was complete, the advancement of the first tunnel on the opposite side of the pile was simulated by deactivating soil elements sequentially for each segment, followed by the activation of the tunnel lining and allowing time for pore pressure dissipation before proceeding. The tunnelling steps were repeated until all segments were completed, as shown in the section "FE Mesh and Boundary Condition.". Finally, after both excavation and tunnelling were finished, the dissipation of remaining excess pore pressure was allowed, and long-term pile settlement was assessed, ensuring that all pressures had dissipated.

3. Interpretation of computed results

3.1 Induced pile settlement due to (a) basement excavation and (b) tunnelling

Fig. 4(a) illustrates the incremental settlement (S_p) of a single pile due to basement excavation in all three cases (i.e., SeSt, TeTt, and BeBt). Excavation depths are indicated by h, which are normalised by the final excavation depth (H_e). Similarly, S_p is normalised by pile diameter (d_p).

It can be seen from Fig. 4(a) that as excavation depth increases, pile settlement increases in all cases. This is attributed to the reduction of shaft resistance and degradation of clay stiffness due to excavation-induced stress release and shear strain. In order to avoid that, the pile had to settle substantially to mobilize end-bearing further. The SeSt case exhibits the least settlement, with a relatively flat curve starting at 0.0356% for a normalized excavation depth (h/H_e) of 0.25, increasing to 0.3999% at h/H_e of 1.0. This minimal settlement is attributed to the lower final excavation depth of 18 m and a low cover-to-diameter ratio (C/D) of 1.5, which results in minimal stress changes and strain, preserving the pile resistance. In contrast, the TeTt case shows a steeper settlement increase, with normalized pile settlement (S_p/d_p) rising from 0.04% at h/H_e of 0.1667 to 1.6692% at h/H_e of 1.0. The BeBt case presents the highest settlement values and steepest curve, increasing sharply from 0.042% at h/H_e of 0.125 to 2.9022% at h/H_e of 1.0. The deep final excavation depth of 36 m and the highest C/D ratio of 3.5 results in substantial stress release and strain, causing a considerable reduction in confining stress and increased shear stress around the pile, significantly reducing the pile resistance to settlement.

Among the three cases discussed, the smallest and largest settlement induced in the pile is in cases SeSt and BeBt. The pile experienced the total settlement (due to working load and excavation) of 13 mm, 24 mm, and 28 mm (i.e., 1.6%, 3%, and 3.5% of pile diameter) in SeSt, TeTt and BeBt, respectively. This settlement behavior is

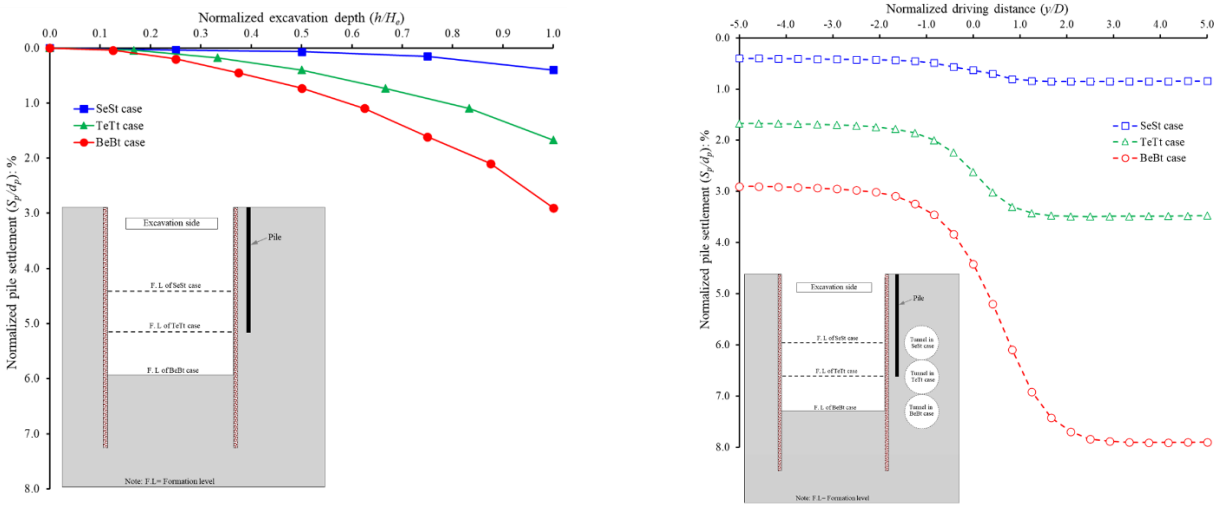

(a) (b)

Fig. 4 Induced pile settlement due to (a) basement excavation and (b) basement excavation and tunnelling

attributed to the more considerable stress relief as the basement excavation goes deeper. In BeBt Case, the pile experiences the highest effective stress release due to excavation. Effective stress release occurs when the soil surrounding the pile undergoes unloading due to excavation, reducing the confining stress around the pile shaft and base. This reduction in stress causes the pile to settle more as it loses some of its lateral support and shaft friction. The effective stress release mechanism is well-documented in the literature. For instance, studies have shown that stress relief around the pile base can lead to additional mobilization of positive shaft friction, which in turn increases settlement (Lee and Ng 2005). Additionally, the reduction in shaft and base resistances due to excavation-induced stress relief can significantly impact the pile capacity, leading to increased settlements (Shi *et al.* 2019).

Fig. 4(b) shows the incremental settlement (S_p) of a single pile due to the combined effect of basement excavation and advancement of the tunnel in all three cases (i.e., SeSt, TeTt, and BeBt). A monitoring section was selected at the transverse centreline of the pile (i.e., y/D = 0) as a reference for the tunnel advancements. The S_p and y are normalised by pile diameter (d_p) and tunnel diameter (D), respectively. It can be seen from the figure that during tunnelling in each case, the induced settlement S_p of the pile is larger than that induced by the excavation alone. This is because of the degradation of stiffness of the clay with tunnelling-induced stress release and shear strain. The stiffness of the ground near the pile was initially degraded by the excavation. Consequently, the tunnelling induced a larger settlement than that of the excavation alone.

The settlement of the pile in all cases increased slightly as the tunnel advanced and approached to pile until the tunnel face reached y/D=-3. However, the rate of induced settlement increased substantially, specifically in TeTt and BeBt cases when the tunnel face reached the monitoring section (y/D=0) and continued to rise until the tunnel reached the y/D=+3. This suggests that the pile was significantly affected when the position of the tunnel face is inside the influence zone, which is 3D behind and 3D in front of the monitoring section. The different influence zones were also reported from the numerical studies conducted by (Lee 2013, Lee and Ng 2005, Mroueh and Shahrour 2002b). Moreover, the SeSt case, with its shallow excavation (12 m) and lower tunnel cover (9 m), experiences minimal disturbance and settlement (0.4% to 0.85%). There are two reasons for this behaviour. First, both excavation and tunnelling activity carried out near the pile shaft induced no disturbance (i.e., shear strain and ground movement) underneath the pile toe. Second, the load carried by the pile shaft is transferred to the pile toe, resulting in the increment of mean effective stress underneath the pile toe. Consequently, the stiffness of the soil element increased. During the tunnelling, the increased soil stiffness underneath the pile toe resulted in negligible settlement. This mechanism is supported by the findings of (Jacobz 2003).

The TeTt case shows increased settlement (1.67% to 3.49%) due to more significant soil displacement and stress redistribution. The BeBt case, with the deepest excavation (24 m) and highest tunnel cover (21 m), exhibits the most severe settlement, reaching up to 7.9%. The combined effect of excavation and tunnelling consistently results in larger pile settlements compared to excavation alone. The reasons for the largest induced settlement in Case BeBt can be tunnelling-induced stress release (which is below the pile toes) and a shear–strain influence zone around the tunnel. This is attributed to the degradation of clay stiffness caused by excavation-induced stress release and shear strain, further exacerbated by the tunnelling process. Moreover, the end-bearing resistance of the pile toe in the BeBt case is reduced due to the stress release below it, causing the pile to move relative to the surrounding ground to mobilize the shaft resistance along the piles. This movement results in increased settlement. This behavior is also seen in the study done by (Shi *et al.* 2019). The total settlement, including working load, basement excavation, and tunnelling effects, varies significantly: 9.2 mm (1.15% of pile diameter) for

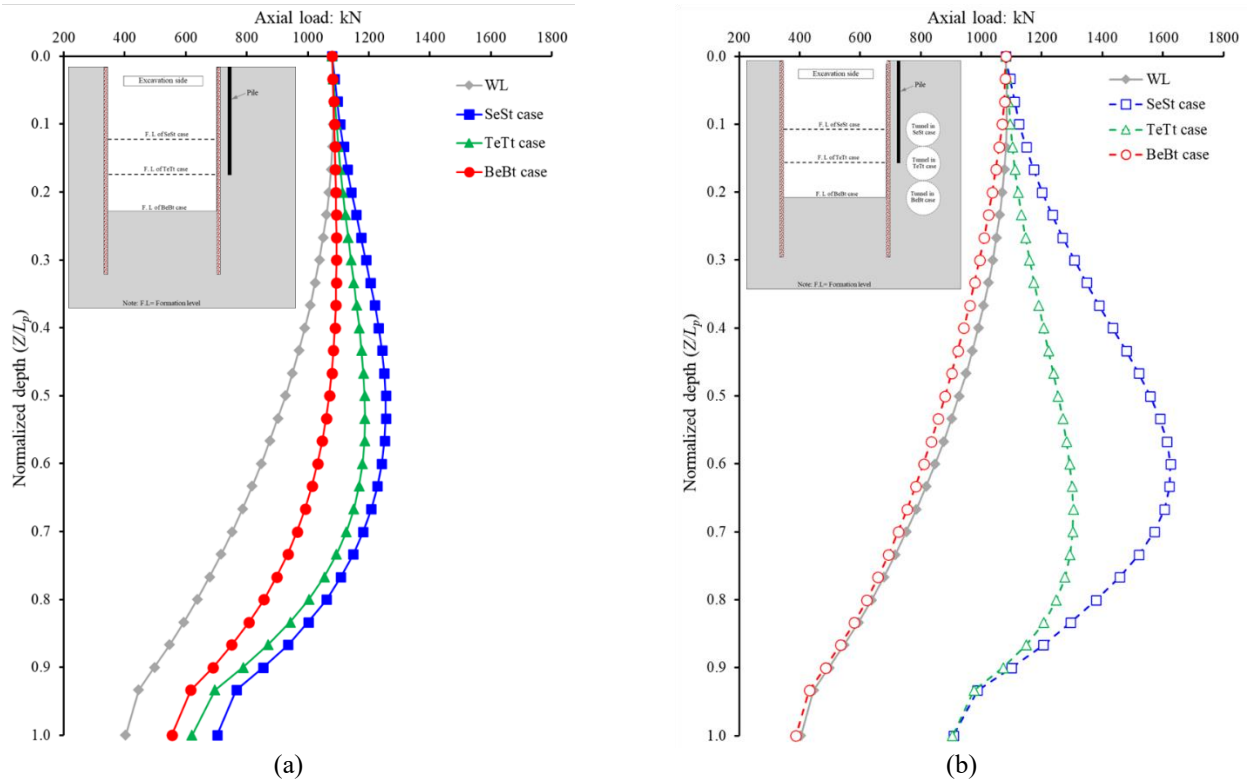

Fig. 5 Axial load distribution along the pile due to (a) basement excavation and (b) basement excavation and tunnelling

SeSt, 30.7 mm (3.8%) for TeTt, and 63.1 mm (7.9%) for BeBt.

3.2 Changes in axial load distribution

Fig. 5(a) illustrates axial load distribution along the pile due to basement excavation and Fig. 5(b) shows axial load distribution along the pile due to the combined effect of basement excavation and advancement of tunnel in all three cases (i.e., SeSt, TeTt, and BeBt). The axial load distribution before excavation and tunnelling (after applying the working load) is also included in the figure as a reference. WL curve shows the axial distribution on the working load. Before the basement excavation and tunnelling, the pile supported approximately 63% of the working load (i.e., 1080 kN) through shaft resistance, while the remaining 37% was carried by end-bearing resistance.

Fig. 5(a) shows that the axial force along the upper portion of the pile increases with depth after basement excavation in each case. This increase is due to the reduction in normal stress on the pile shaft, which causes a reduction in shaft resistance—a trend consistently observed across all cases. However, this pattern does not remain consistent after the combined basement excavation and tunnelling in BeBt case.

In the SeSt case, basement excavation was initially conducted near the mid-depth of the pile shaft, resulting in a decrease in shaft resistance due to the reduction in normal stress on the pile shaft. As a consequence, the axial stress increased with depth, with the maximum axial load observed at a normalized depth of Z/L_p=0.53. At this depth, the axial load increased by 16% compared to the working load (i.e., 1080 kN). This axial load distribution indicates that the shaft resistance in the upper portion of the pile decreases up to Z/L_p=0.53, leading to a transfer of load to the lower portion. (Zheng *et al.* 2012) observed similar mechanisms of load transfer. To maintain equilibrium, the pile had to settle (can be seen in Fig. 4), thereby mobilizing both the shaft resistance and end-bearing resistance along the lower portion of the pile (i.e., Z/L_p > 0.53). This process resulted in increases of 74% and 10% in the mobilized end-bearing and shaft resistance at the lower portion, respectively, compared to the conditions before excavation. The tunnelling after the basement excavation, in this case caused a further reduction of the normal stresses to the pile shaft as shown in Fig. 5(b). Consequently, soil settled more than the pile (discussed in Section 3.3), resulting in negative skin friction (NSF) along the upper half of the pile ($Z/L_p \leq 0.6$) and this NSF is evidenced by (Lee and Ng 2005). The maximum axial load, which showed a 50% increase compared to the working load, was observed at a depth of Z/L_p=0.6. This suggests that this portion of the pile is subjected to "dragload" by the surrounding soil. This caused the pile to settle more than that due to the basement excavation alone (see Fig. 4). To maintain the vertical equilibrium of the pile, the soil surrounding the lower part of the pile (Z/L_p>0.6) resisted its settlement by mobilizing positive skin friction (PSF) at the pile-soil interface and end-bearing resistance at the toe of the pile. This mechanism of PSF was also observed in (Lee and Ng 2005). Owing to the combined basement excavation and tunnelling, the end-bearing and mobilised shaft resistance increased to 125% and 61%, respectively.

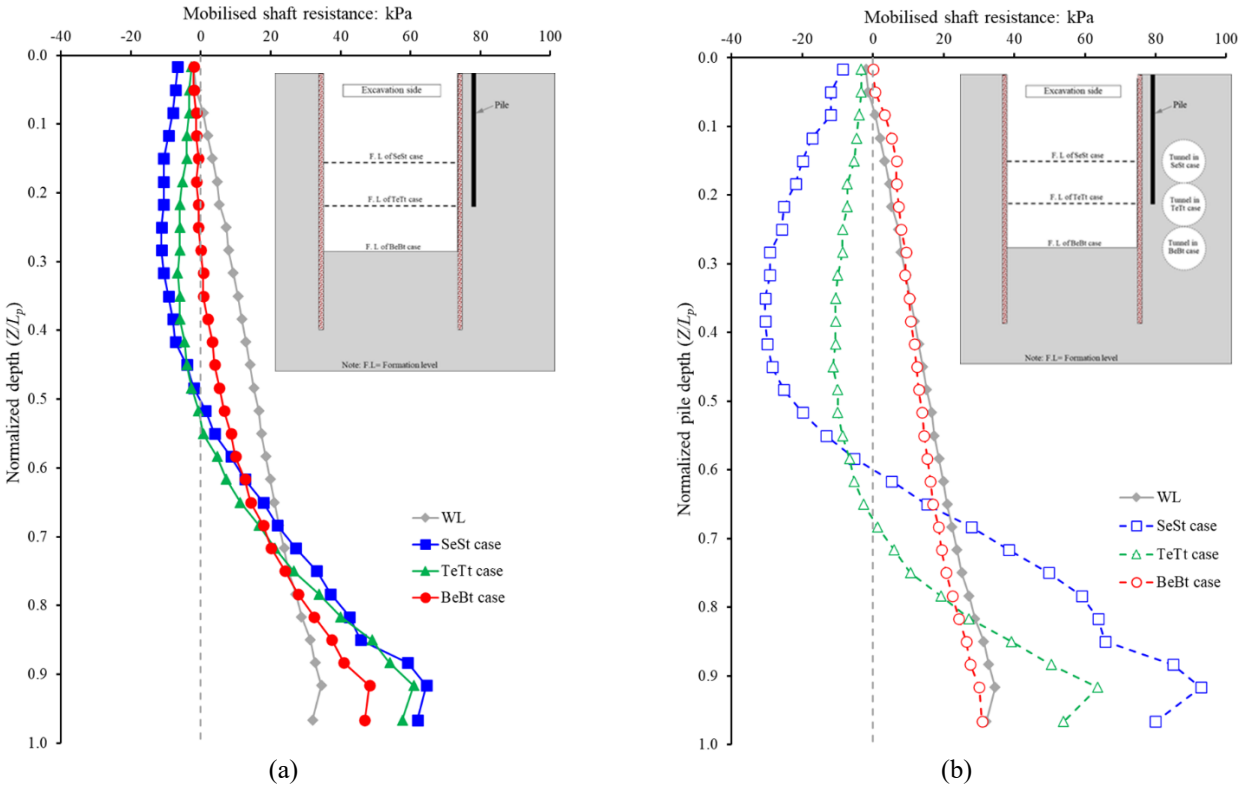

Fig. 6 Mobilized shaft resistance along the pile length after completion of (a) basement excavation and (b) basement excavation and tunnelling

In the TeTt case, the axial load increased along the pile up to a normalized depth of Z/L_p=0.533, following a pattern similar to that observed in the SeSt case. Additionally, after tunnelling in the TeTt case, the axial load continued to increase up to a depth of Z/L_p=0.66, reflecting the behavior seen in the SeSt case. The maximum increase in axial load compared to the working load was observed at these locations to be 9.9% after basement excavation and 20.7% after tunnelling. The increase in axial load resulted from the reduced shaft resistance, as discussed in Section 3.3, which was caused by stress release due to combined excavation and tunnelling carried out near the pile toe. Consequently, the axial load was transferred to the lower portion of the pile, resulting in a 124.4% increase in toe resistance and a 4.26% increase in shaft resistance after the combined effects of basement excavation and tunnelling. (Shi *et al.* 2019) also observed similar behaviour. In this case, the pile had to settle more compared to the SeSt case, and a greater reduction in mobilized shaft resistance was observed compared to the SeSt scenario.

In contrast to the case SeSt and TeTt, there is slight increase in axial load in the upper part of the pile after excavation ($Z/L_p \leq$ 0.3) with maximum increase of 1.3% as compared to the applied working load in the BeBt case. Afterwards, a significant decrease in axial load was observed. This indicates that the load was transferred to the pile lower part. In this case, the pile settles substantially to mobilise the end-bearing resistance after basement excavation. Therefore, there is an increase in end bearing resistance of 37.5%, while 15% reduction in the shaft resistance was observed at the end of basement excavation as compared to before excavation and tunnelling. (Hsiung 2009) also reported an increase and decrease in the end bearing and shaft resistance, respectively. However, with the advancement of the tunnel, the axial load decreased along the entire length of the pile. This advancement of tunnel led to a reduction of 3.9% in the end bearing resistance while increase in shaft resistance of 2.3%. As a larger reduction rate of the axial load along the depth corresponds to a relative shaft resistance, significant shaft resistance is mobilized along the entire pile shaft to maintain the vertical force equilibrium, accompanied by the continuous settlement of the pile (can be seen in Fig. 4).

3.3 Mobilised shaft resistance on completion of basement excavation and tunnelling

To substantiate the discussion in the previous section, the mobilised shaft resistance in the pile after the application of the working load (i.e., before basement excavation and tunnelling) is shown in Fig. 6. In the figure, the depth below the ground surface (Z) is normalised by the pile length (L_p). The computed average mobilised unit shaft resistance $f(Z)$ at various depths was calculated based on the following equation

$$f(Z) = \frac{\Delta Q_{(Z)}}{s.\Delta Z} \quad (2)$$

where ΔQ is the difference between the computed axial loads at two consecutive depths, ΔZ is the vertical distance between the two consecutive depths, and s is the perimeter of the pile.

It can be seen from Fig. 6 that after applying the working load, positive shaft resistance is mobilized progressively along the entire length of the pile, consistent with typical pile behavior in stiff soils. As the pile depth increases, the mobilized shaft resistance continues to rise steadily after the working load. The shaft resistance peaks at 34.57 kPa near the toe of the pile, at a normalized depth of approximately Z/L_p=0.917, before slightly decreasing at the very end. This indicates that at the end of the pile, the load is primarily resisted by the pile toe.

On the completion of the basement excavation in SeSt case, the shaft resistance decreased to zero in the upper portion (Z/L_p<0.5) of the pile while increased in lower portion (Z/L_p≥0.5) of the pile. This computed distribution of mobilised shaft resistance is similar to that measured from centrifuge tests by (Chiang and Lee 2007). The reason for this behaviour is that there is a reduction in normal stress in the upper part of the pile due to the basement excavation. In the result, load is transferred to the lower part of the pile (Fig 5). Tunnelling after the basement excavation in this case caused negative skin friction (NSF) mobilisation at the upper part of the pile shaft (0 ≤Z/L_p≤0.6) due to stress release and soil movement. (Zheng *et al*. 2012) has also reported the development of negative skin friction in the upper part of the pile. This implies that this portion of the pile is 'dragged' down by the surrounding soil, which settles due to tunnelling. To maintain vertical equilibrium of the pile, the soil surrounding the upper part of the pile resists it from settling by mobilising PSF at the soil–pile interface. The neutral plane, where the zero-shaft resistance is mobilised, is located at a depth of Z/L_p=0.6. This location is consistent with the depth where the maximum axial load was induced (see Fig. 4). Consequently, an additional load was transferred to the lower part of the pile. This is also supported by centrifuge tests conducted by (Chiang and Lee 2007) who found that an increase in load results in a downward shift of the neutral plane due to increased dragload. To support the applied working load and "dragload" resulting from NSF, the pile settled substantially to mobilise its end-bearing resistance (see Fig. 5).

In the TeTt case, basement excavation and tunnelling near the pile toe similarly resulted in a reduction in shaft resistance in the upper portion of the pile and an increase in the lower portion. However, the reduction in normal stresses on the pile shaft was more significant due to stress release when compared to the SeSt case. As a result, the pile experienced greater settlement to accommodate the vertical load, leading to a higher mobilization of end-bearing resistance relative to shaft resistance. Furthermore, the neutral plane shifted slightly more downward, occurring at Z/L_p=0.67 in the TeTt case, compared to Z/L_p=0.6 in the SeSt case after basement excavation and tunnelling. This downward shift is attributed to the increase in dragload caused by negative skin friction. According to Hong *et al*. (2025), an increase in load results in a downward shift of the neutral plane.

In contrast to the SeSt and TeTt cases, following the basement excavation and tunnelling, the shaft resistance in the BeBt case exhibited a steady increase along the entire depth of the pile (0≤Z/L_p≤1). This increase occurred alongside a continuous decrease in axial load (as illustrated in Fig. 5) and was accompanied by ongoing settlement of the pile (as shown in Fig. 4). The rise in shaft resistance was driven by the significant settlement, which was greater than that observed in the SeSt and TeTt cases. This settlement was a result of reduced end-bearing capacity due to stress relief beneath the pile toe due to basement excavation and tunnelling. Consequently, there was a 3.9% reduction in end-bearing resistance, while shaft resistance increased by 2.3% at the base of the pile. The increased mobilization of shaft resistance along the pile in the BeBt case and the reduced end-bearing capacity are similar to the behavior of floating piles studied by (Zheng *et al*. 2012). They observed that, under stress relief, end-bearing piles show a reduction in axial load near the pile toe, leading to higher mobilization of shaft resistance to maintain equilibrium.

3.4 Induced bending moment in the pile

Fig. 7 presents the distribution of induced bending moments along the pile resulting from basement excavation and the combined effects of basement excavation and tunnelling for the SeSt, TeTt, and BeBt cases. A positive bending moment indicates that tensile stress was induced along the pile shaft facing the basement excavation. Given that the pile head was not rigidly constrained (i.e., it was free to move and rotate), no significant bending moment was observed at or near the pile head across all cases, and the same is discussed by (Liyanapathirana and Nishanthan, 2016).

In the SeSt case, the excavation leads to an increase in bending moments with depth, reaching a maximum value near the middle of the pile, as illustrated in Fig. 7(a). The maximum bending moment after basement excavation was computed approximately 194.2 kNm at a depth of Z/L_p=0.6, which represents 25.8% of the pile bending moment capacity. This suggests that stress release due to excavation caused lateral soil movement towards the excavation side. However, when tunnelling is introduced, there is a distinct shift in the bending moment profile, as shown in Fig. 7(b). The tunnelling process induces a positive bending moment in the uppermost part of the pile (0≤Z/L_p≤0.4) and the lowermost part (0.8≤Z/L_p≤1), while a negative bending moment is observed in the middle portion of the pile (0.4<Z/L_p<0.8). This pattern is attributed to stress release on the opposite side of the pile due to tunnelling near the mid-depth of the pile shaft. This trend is consistent with the study done (Ng *et al*. 2013). To counterbalance this induced negative bending moment, positive bending moments developed along the uppermost and lowermost sections of the pile. The maximum positive and negative bending moment was observed at 49 kNm and 181 kNm, respectively, after the combined basement excavation and tunnelling. Thus, it can be concluded that the overall bending moments in the pile are reduced after the tunnelling phase.

In the TeTt case, Initially, during the excavamtion phase, the bending moment increases with depth, like the SeSt case. The maximum bending moment after basement excavation occurs at a depth of Z/L_p=0.633, where it reaches approximately 248.7 kNm, representing 33.0% of the pile bending moment capacity. This indicates a significant stress release due to excavation, leading to lateral soil movement toward the excavation. This lateral soil movement towards

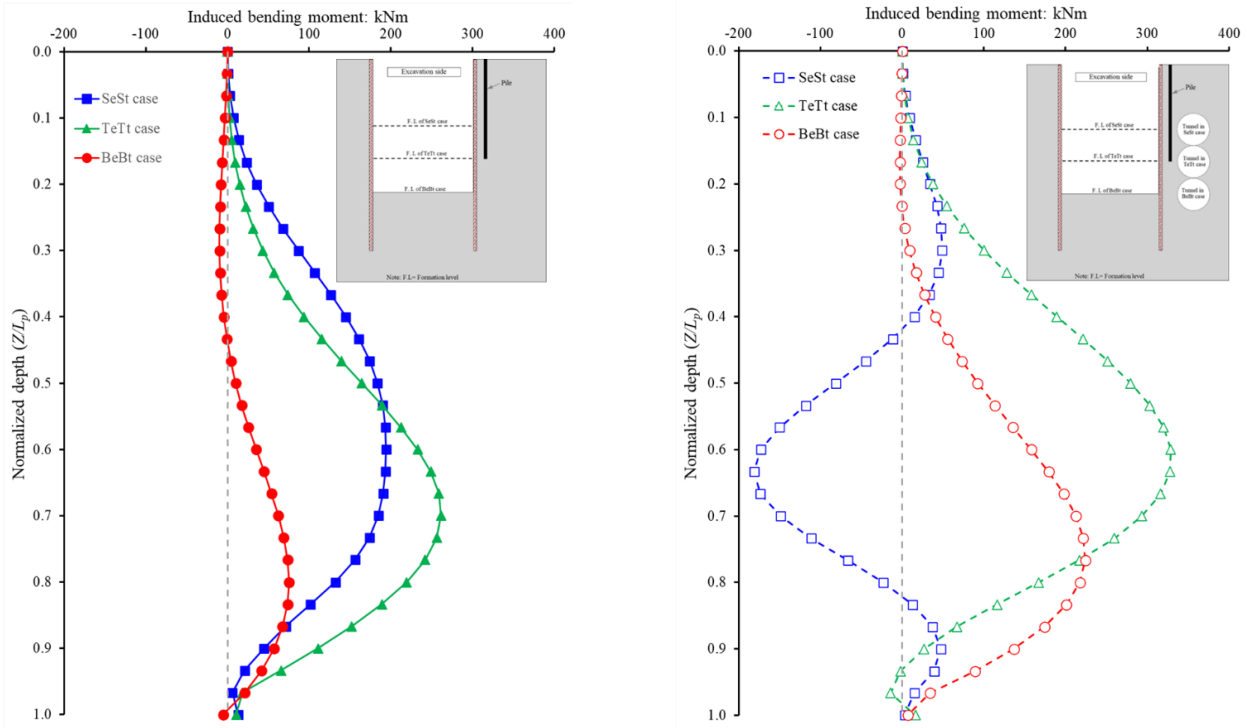

Fig. 7 Induced bending moment along the pile in all the three tests during (a) basement excavation and (b) basement excavation and tunnelling process

the excavation, as observed in both cases SeSt and TeTt cases, was also noted by (Shi *et al.* 2019). Similar to the SeSt case, tunnelling significantly affects the bending moments, reducing their magnitude near the surface while increasing compressive stresses (negative bending moment) at the lower sections of the pile. The stress profile remains somewhat similar to the SeSt case, but the overall magnitude is higher, indicating a more pronounced impact of both excavation and tunnelling on the pile structural behavior in the TeTt case. The maximum positive bending moment was 328 kNm after combined excavation and tunnelling, which is 43.7% of pile bending moment capacity.

The BeBt case presents a different bending moment distribution profile compared to the SeSt and TeTt cases. The bending moments are generally lower, with a maximum positive moment of 75.42 after basement excavation occurring near the pile bottom at Z/L_p=0.8. In addition, there were slightly negative bending was computed at the upper part of the pile ($0 \leq Z/L_p \leq 0.43$).

When tunnelling was introduced, the positive bending moment increased with a maximum value of 224 kNm (that was approx. 30% of piles bending moment capacity) at Z/L_p=0.75.

In conclusion, the analysis of induced bending moments from basement excavation and tunnelling across the SeSt, TeTt, and BeBt cases demonstrate varying impacts on pile behavior. While the BeBt case exhibited the lowest bending moments after basement excavation, the subsequent tunnelling resulted in higher bending moments than SeSt but still lower than TeTt. This indicates that combined excavation and tunnelling significantly influence pile behavior, particularly in the TeTt scenario, where the maximum bending moments are observed. Similar to my findings, (Soomro *et al.* 2017) also noted that twin tunnelling causes the development of positive and negative bending moments along the pile shaft after tunnelling on both sides of a pile.

The analysis indicates that the maximum induced bending moments at the end of excavation in all three cases remain below the pile bending moment capacity of 750 kNm. Consequently, the primary concern in the excavation-tunnelling-soil-pile interaction is the potential for significant settlement and lateral displacement of the pile. However, this conclusion may not be universally applicable, as variations in ground conditions or the stiffness of the excavation systems such as wall and prop stiffness—could lead to different behaviors. Thus, further research is needed to validate these findings under diverse conditions and configurations.

3.5 Pile defection

To provide further support for the discussion presented in the previous section, this section delves into the interpretation of induced pile deflection.

Figs. 8(a) and 8(b) illustrate the normalized deflection (x/d_p%) along the normalized pile length (Z/L_p), resulting from basement excavation alone and from the combined effects of basement excavation and tunnelling, respectively. In these figures, positive values indicate that the pile deflected toward the side of the basement excavation. The figure clearly demonstrates that following the basement

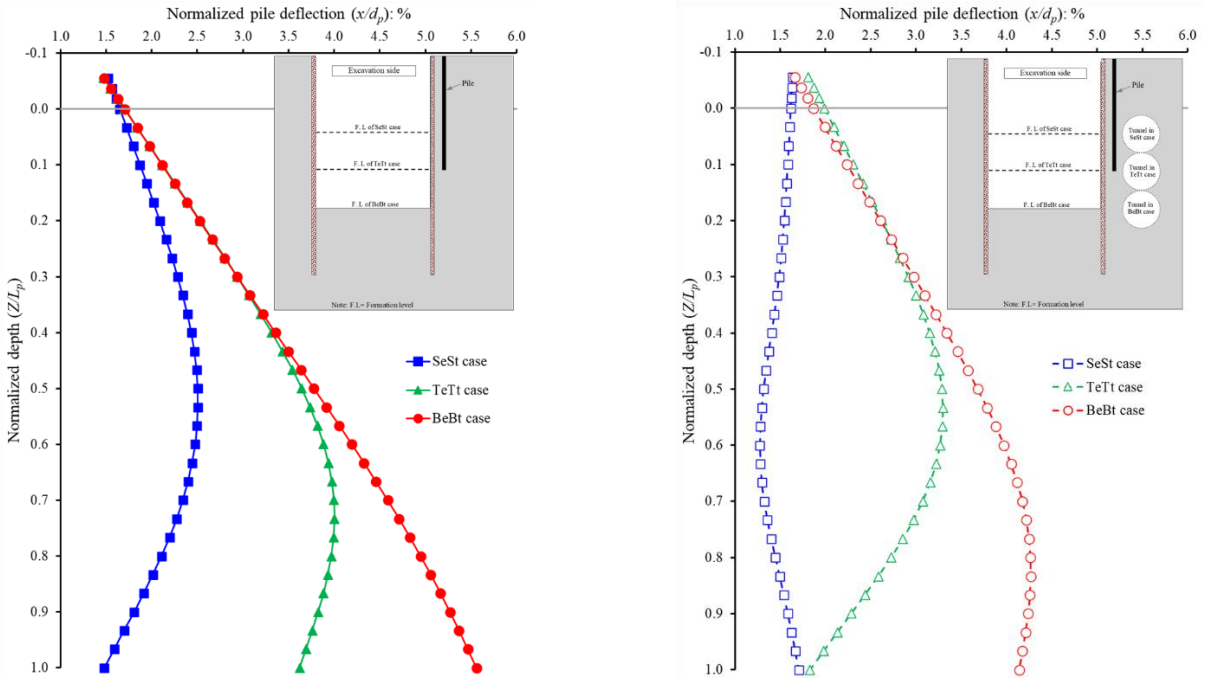

Fig. 8 Induced pile deflection of all cases after completion of (a) basement excavation and (b) basement excavation and tunnelling process

excavation, the pile deflects towards the excavation in all cases. This behavior indicates a consistent pattern of pile response to the excavation process, highlighting the influence of excavation-related stress changes on pile deflection. The similar observation was noted by (Soomro *et al.* 2019). The observed deflection towards the excavation suggests that the removal of soil contributes to stress relief and resultant bending moments on the pile, leading to this characteristic deformation as evidenced by (Hsiung 2009, Shi *et al.* 2019)

From the figures, it is evident that in the SeSt case, during basement excavation, the middle portion of the pile experiences greater deflection compared to both the upper and lower portions. The pile deflection gradually increases along the pile length, with a maximum deflection value of 2.50% at Z/L_p=0.533, which is near the midpoint of the pile. This pronounced deflection is attributed to the release of soil stress on the excavation side, which causes soil on the opposite side to flow toward the excavation. Beyond this maximum deflection point, the deflection decreases toward the lower portion of the pile, with values decreasing to 1.48% at the pile toe—nearly matching the deflection at the pile head (1.52%). The trend closely aligns with the study done by (Leung *et al.* 2000), who conducted centrifuge tests to investigate the effects of excavation-induced soil movements on nearby piles and observed maximum deflection near the pile midpoint. However, when tunnelling is introduced following the excavation, there is a subsequent release of stress on the side opposite the excavation. This stress relief causes the pile to return to an almost original position. This suggests that the middle portion of the pile is more susceptible to deflection during basement excavation. Nevertheless, it is observed that the deflection values at both the pile head and toe due to the combined effects of basement excavation and tunnelling are slightly higher than those observed for basement excavation alone.

In the TeTt case, the pile deflection exhibits a pattern similar to that observed in the SeSt case following the basement excavation. However, the deflection is more uniformly distributed along the length of the pile in the TeTt scenario and is also more pronounced. The maximum deflection recorded in the TeTt case was 4.0% at a depth ratio (Z/L_p) of 0.733, which exceeds the maximum deflection observed in the SeSt case. This increased deflection can be attributed to a greater stress release resulting from a deeper basement excavation. Subsequently, the deflection decreases along the pile length, with a value of 3.6% at the pile toe, which is also higher than the corresponding value in the SeSt case. In contrast, after tunnelling, the behavior of the pile in the TeTt case differs from that in the SeSt case; specifically, the pile does not fully recover to its original position. The maximum deflection recorded in the TeTt case after tunnelling was 3.2984% at Z/L_p = 0.55, indicating a redistribution of stress along the pile and a release of soil stress on the tunnelling side. This deflection continues to decrease along the pile length, reaching a minimum value of 1.8% at the pile toe, although this value remains higher than that measured in the SeSt case.

In contrast to the SeSt and TeTt case, during basement excavation alone, the pile exhibits a linear increase in deflection along its length, with the maximum deflection of 5.56% occurring at the pile toe in the BeBt Case. This is because of excavation-induced effective stress release and soil displacement towards excavation. This increasing trend

suggests that the pile is progressively affected by the stress release due to excavation, with the toe region being particularly vulnerable.

The maximum deflection in the BeBt case (5.56%) at pile toe is notably higher than in both the SeSt and TeTt cases, reflecting the more pronounced impact of the depth of basement excavation on the pile.

When tunneling is introduced after the basement excavation, the deflection behavior changes. The combined effects cause the pile deflection to decrease compared to the deflection due to basement excavation alone, particularly toward the lower portion of the pile. The maximum deflection reduces to 4.15% at the pile toe, which is a significant decrease from the 5.56% observed during basement excavation alone. However, it is important to note that this deflection remains greater than the values recorded in the SeSt and TeTt cases. This observed reduction in deflection can be attributed to the redistribution of stresses induced by tunnelling. As tunnelling relieves stress beneath the pile toe, it facilitates a partial recovery of the pile from the deflection caused by the earlier excavation activities. This mechanism highlights the interplay between excavation and tunnelling processes and their collective influence on pile behavior.

In comparing the SeSt, TeTt, and BeBt cases, distinct pile deflection patterns emerge during excavation. The SeSt case shows greater deflection in the middle of the pile, while the TeTt case has a more uniform and pronounced profile due to deeper excavation. The BeBt case features a linear increase, with the largest deflection at the pile toe. Following tunnelling, the SeSt case partially recovers, but the TeTt case does not fully return to its original state. Overall, the BeBt case exhibits the highest deflection values, highlighting the effect of basement excavation-tunnelling on pile behavior.

4. Conclusions

This research explores the response of a single pile to the sequential effects of basement excavation and tunnelling in stiff clay, employing three-dimensional coupled consolidation numerical modelling. This parametric study examined three basement excavation depths and tunnel positions relative to the pile, including scenarios near the pile shaft (SeSt), near the pile toe (TeTt), and below the pile toe (BeBt), with tunneling simulated after excavation. In each scenario, the tunnel excavation was simulated after the basement excavation. Based on the computed results, the following conclusions were drawn:

- Basement excavation followed by tunneling caused significantly greater pile settlements than excavation alone, with the highest settlement of 63.1 mm (7.9% of pile diameter) occurring in the BeBt case and the lowest of 9.2 mm (1.15%) in the SeSt case. These settlements resulted from stress release and shear strain, which degraded clay stiffness and reduced shaft resistance, requiring additional pile settlement to mobilize end-bearing resistance.
- Axial load distribution increases along the pile after basement excavation due to stress release, with SeSt and TeTt cases showing higher loads in the upper pile and transfer to the lower portion. Tunneling further increase loads at upper pile portion through negative skin friction and mobilizes resistance at the lower portion of the pile, with SeSt showing the largest increase (50%), while BeBt exhibits a significant re-distribution of shaft resistance to maintain equilibrium.
- Basement excavation induced maximum bending moments near the middle of the pile, with the SeSt case reaching 194.2 kNm and the TeTt case experiencing a higher 248.7 kNm due to pronounced lateral soil movement. Tunneling further increased bending moments, with the TeTt case showing the highest positive bending moment of 328 kNm, while the BeBt case exhibited the lowest moments overall but higher values than SeSt after tunneling.
- Following basement excavation, piles deflected towards the excavation in all cases, with the SeSt case showing a maximum deflection of 2.50% at mid-depth, nearly recovering after tunneling. In contrast, the TeTt and BeBt cases exhibited greater deflections, with maximum values of 4.0% and 5.56%, respectively, with partial recovery after tunneling.

Future research could explore the effects of sequential basement excavation and tunneling on piles in different soil types, such as soft clay and sand. Additionally, field monitoring and advanced constitutive models can further enhance the understanding of soil-pile interaction under varying geotechnical conditions.

Acknowledgments

The authors would like to acknowledge the funding support from the Joint Fund for Railway Basic Research of China (Grant No. U2268213).

References

Abrams, A.J. (2007), Earth pressure balance (EPB) tunneling induced settlements in the Tren Urbano Project, Rio Piedras, Puerto Rico.

Al Tabbaa, A. (1987), Permeability and stress-strain response of speswhite kaolin.

Benz, T. (2007), "Small strain stiffness of soils and its numerical consequences", Ph. D. Dissertation, Universitat Stuttgart, 187.

Bezuijen, A. and van der Schrier, J. (1994), "The influence of a bored tunnel on pile foundations BT - Centrifuge '94", *Proceedings of the international conference*, (Eds., C.F. Leung, F.H. Lee and T.S. Tan), 681-686. Balkema.

Bolton, M.D. (1986), "The strength and dilatancy of sands", *Géotechnique*, **36**(1), 65-78. https://doi.org/10.1680/geot.1986.36.1.65.

Boonyarak, T. and Ng, C.W.W. (2014), "Effects of construction sequence and cover depth on crossing-tunnel interaction", *Can. Geotech. J.*, **52**(7), 851-867. https://doi.org/10.1139/cgj-2014-0235.

Cheng, C.Y., Dasari, G.R., Chow, Y.K. and Leung, C.F. (2007), "Finite element analysis of tunnel-soil-pile interaction using displacement controlled model", *Tunn. Undergr. Sp. Tech.*, **22**(4), 450-466. https://doi.org/10.1016/j.tust.2006.08.002.

Chiang, K.H. and Lee, C.J. (2007), "Responses of single piles to tunneling-induced soil movements in sandy ground", *Can. Geotech. J.*, **44**(10), 1224-1241. https://doi.org/10.1139/T07-050.

Cui, C., Meng, K., Xu, C., Liang, Z., Li, H. and Pei, H. (2021), "Analytical solution for longitudinal vibration of a floating pile in saturated porous media based on a fictitious saturated soil pile model", *Comput. Geotech.*, **131**, 103942. https://doi.org/10.1016/j.compgeo.2020.103942.

Ding, Z., Wei, X.J. and Wei, G. (2017), "Prediction methods on tunnel-excavation induced surface settlement around adjacent building", *Geomech. Eng.*, **12**(2), 185-195. https://doi.org/10.12989/gae.2017.12.2.185.

Fang, J., Lin, S. and Liu, K. (2023), "Multi-scale study of load-bearing mechanism of uplift piles based on model tests and numerical simulations", *Scientific Reports*, **13**(1), 6410. https://doi.org/10.1038/s41598-023-33221-z.

Finno, R.J., Lawrence, S.A., Allawh, N.F. and Harahap, I.S. (1991), "Analysis of performance of pile groups adjacent to deep excavation", *J. Geotech. Eng.*, **117**(6), 934-955. https://doi.org/10.1061/(ASCE)0733-9410(1991)117:6(934).

Goh, A.T.C., Wong, K.S., Teh, C.I. and Wen, D. (2003), "Pile response adjacent to braced excavation", *J. Geotech. Geoenviron. Eng.*, **129**(4), 383-386. https://doi.org/10.1061/(ASCE)1090-0241(2003)129:4(383).

Herle, I. and Gudehus, G. (1999), "Determination of parameters of a hypoplastic constitutive model from properties of grain assemblies", *Mech. Cohesive-Frictional Mater.*, **4**(5), 461-486. https://doi.org/10.1002/(sici)1099-1484(199909)4:5<461::aid-cfm71>3.0.co;2-p.

Hong, Y., He, B., Wang, L.Z., Wang, Z., Ng, C.W.W. and Mašín, D. (2017), "Cyclic lateral response and failure mechanisms of semi-rigid pile in soft clay: centrifuge tests and numerical modelling", *Can. Geotech. J.*, **54**(6), 806-824. https://doi.org/10.1139/cgj-2016-0356.

Hong, Y., Zhang, J.F., Wang, L.Z. and Liu, T. (2020), "On evolving size and shape of gas bubble in marine clay under multi-stage loadings: microcomputed tomography (μCT) characterization and cavity contraction analysis", *Can. Geotech. J.*, **57**(7), 1072-1091. https://doi.org/10.1139/cgj-2019-0076.

Hong, Yi, Wang, L., Yang, B. and Zhang, J. (2019), "Stress-dilatancy behaviour of bubbled fine-grained sediments", *Eng. Geol.*, **260**, 105196. https://doi.org/10.1016/j.enggeo.2019.105196.

Hsiung, B.C.B. (2009), "A case study on the behaviour of a deep excavation in sand", *Comput. Geotech.*, **36**(4), 665-675. https://doi.org/10.1016/j.compgeo.2008.10.003.

Jacobz, S.W. (2003), "Tunnelling effects on piled foundations", *Tunn. Tunn. Int.*, **35**(6), 28–31. https://doi.org/NA

Jeon, Y.J. and Lee, C.J. (2023), "Analysis of pile group behaviour to adjacent tunnelling considering ground reinforcement conditions with assessment of stability of superstructures", *Geomech. Eng.*, **33**(5), 463-475. https://doi.org/10.12989/gae.2023.33.5.463.

Jeon, Y.J., Seo, S.K., Choi, Y.N., Son, H.Y., Park, B.S., Kim, J.H. and Lee, C.J. (2024), "Effects of pile tip cutting due to shield TBM tunnel construction on pile behaviour under various reinforcement conditions", *Geomech. Eng.*, **39**(2), 181-195. https://doi.org/10.12989/gae.2024.39.2.181.

Kim, S.B., Oh, D.W., Cho, H.J. and Lee, Y.J. (2024), "Investigation of pile group response to adjacent twin tunnel excavation utilizing machine learning", *Geomech. Eng.*, **38**(5), 517-528. https://doi.org/10.12989/gae.2024.38.5.517.

Kolymbas, D. (1991), "An outline of hypoplasticity", *Arch. Appl. Mech.*, **61**(3), 143-151. https://doi.org/10.1007/bf00788048.

Korff, M., Mair, R.J. and Van Tol, F.A.F. (2016), "Pile-soil interaction and settlement effects induced by deep excavations", *J. Geotech. Geoenviron. Eng.*, 142(8), 04016034-NA. https://doi.org/10.1061/(ASCE)GT.1943-5606.0001434.

Lee, C.J. (2013), "Numerical analysis of pile response to open face tunnelling in stiff clay", *Comput. Geotech.*, **51**(51), 116-127. https://doi.org/10.1016/j.compgeo.2013.02.007.

Lee, G. and Ng, C.W.W. (2005), "Effects of advancing open face tunneling on an existing loaded pile", *J. Geotech. Geoenviron. Eng.*, **131**(2), 193-201. https://doi.org/10.1061/(ASCE)1090-0241(2005)131:2(193).

Leung, C.F., Chow, Y.K. and Shen, R.F. (2000), "Behavior of pile subject to excavation-induced soil movement", *J. Geotech. Geoenviron. Eng.*, **126**(11), 947-954. https://doi.org/10.1061/(ASCE)1090-0241(2000)126:11(947).

Lim, C.B., Jusoh, S.N., Lim, C.X., Abang Hasbollah, D.Z. and Sohaei, H. (2023), "Tunnel – pile interaction sequence: Parametric studies", *Phys. Chem. Earth*, **129**. https://doi.org/10.1016/j.pce.2022.103312.

Liu, M., Meng, F., Chen, R., Cheng, H. and Li, Z. (2023), "Numerical study on the lateral soil arching effect and associated tunnel responses behind braced excavation in clayey ground", *Transport. Geotech.*, **40**, 100970. https://doi.org/10.1016/j.trgeo.2023.100970.

Liyanapathirana, D.S. and Nishanthan, R. (2016), "Influence of deep excavation induced ground movements on adjacent piles", *Tunn. Undergr. Sp. Tech.*, **52**, 168-181. https://doi.org/10.1016/j.tust.2015.11.019.

Loganathan, N., Poulos, H.G. and Stewart, D.P. (2000), "Centrifuge model testing of tunnelling-induced ground and pile deformations", *Géotechnique*, **50**(3), 283-294. https://doi.org/10.1680/geot.2000.50.3.283.

Mair R.N. and Taylor, R.N. (1997), Bored tunnelling in the urban environment (State-of-the-art report and theme lecture).

Mašín, D. (2005), "A hypoplastic constitutive model for clays", *Int. J. Numer. Anal. Method. Geomech.*, **29**(4), 311-336. https://doi.org/10.1002/nag.416.

Mašín, D. and Herle, I. (2005), "State boundary surface of a hypoplastic model for clays", *Comput. Geotech.*, **32**(6), 400-410. https://doi.org/10.1016/j.compgeo.2005.09.001.

Mayne, P.W. and Kulhawy, F.H. (1982), "K_o - OCR relationships in soil", *J. Geotech. Eng. Division*, **108**(6), 851-872. https://doi.org/10.1061/AJGEB6.0001306.

Mroueh, H. and Shahrour, I. (2002a), "Three-dimensional finite element analysis of the interaction between tunneling and pile foundations", *Int. J. Numer. Anal. Method. Geomech.*, **26**(3), 217-230. https://doi.org/10.1002/nag.194.

Mroueh, H. and Shahrour, I. (2002b), "Three-dimensional finite element analysis of the interaction between tunneling and pile foundations", *Int. J. Numer. Anal. Method. Geomech.*, **26**(3), 217-230. https://doi.org/10.1002/nag.194.

Mroueh, H. and Shahrour, I. (2003), "A full 3-D finite element analysis of tunneling–adjacent structures interaction", *Comput. Geotech.*, **30**(3), 245-253. https://doi.org/10.1016/s0266-352x(02)00047-2.

Ng, C.W.W., Lu, H. and Peng, S.Y. (2013), "Three-dimensional centrifuge modelling of the effects of twin tunnelling on an existing pile", *Tunn. Undergr. Sp. Tech.*, **35**, 189-199. https://doi.org/10.1016/j.tust.2012.07.008.

Ng, C.W.W., Yau, T.L.Y., Li, J.H.M. and Tang, W.H. (2001), "New failure load criterion for large diameter bored piles in weathered geomaterials", *J. Geotech. Geoenviron. Eng.*, **127**(6), 488-498. https://doi.org/10.1061/(ASCE)1090-0241(2001)127:6(488).

Niemunis, A. and Herle, I. (1997), "Hypoplastic model for cohesionless soils with elastic strain range", *Mech. Cohesive-frictional Mater.*, **2**(4), 279-299. https://doi.org/10.1002/(SICI)10991484(199710)2:4<279::AID-CFM29>3.0.CO;2-8.

Ong, C.W., Leung, C.F., Yong, K.Y. and Chow, Y.K. (2006), *Pile responses due to tunnelling in clay*.

Pang, C., Chow, Y. and Yong, K. (2005), Three-dimensional numerical simulation of tunnel advancement on adjacent pile foundation. In *Underground Space Use. Analysis of the Past and Lessons for the Future*, Taylor & Francis. https://doi.org/10.1201/NOE0415374521.ch171.

Parry, R.H.G. and Nadarajah, V. (1974), "Observations on laboratory prepared, lightly overconsolidated specimens of kaolin", *Géotechnique*, **24**(3), 345-357. https://doi.org/10.1680/geot.1974.24.3.345.

Poulos, H.G. and Chen, L.T. (1996), "Pile response due to unsupported excavation-induced lateral soil movement", *Can. Geotech. J.*, **33**(4), 670-677. https://doi.org/10.1139/t96-091-312.

Poulos, H.G. and Chen, L.T. (1997), "Pile response due to excavation-induced lateral soil movement", *J. Geotech. Geoenviron. Eng.*, **123**(2), 94-99. https://doi.org/10.1061/(ASCE)1090-0241(1997)123:2(94).

Shaaban, M.G.I., Kenawi, M.A., Senoon, A.A.A. and El-Naiem, M.A.A. (2023), "Effects of excavation and construction sequence on behavior of existing pile groups", *Innov. Infrastruct. Solutions*, **8**(8), 1-12. https://doi.org/10.1007/s41062-023-01193-8.

Shi, J., Wang, J., Chen, Y., Shi, C., Lu, H., Ma, S. and Fan, Y. (2023), "Physical tung of the influence of tunnel active face instability on existing pipelines", *Tunn. Undergr. Sp. Tech.*, **140**, 105281. https://doi.org/10.1016/j.tust.2023.105281.

Shi, J., Wei, J., Ng, C.W.W. and Lu, H. (2019), "Stress transfer mechanisms and settlement of a floating pile due to adjacent multi-propped deep excavation in dry sand", *Comput. Geotech.*, **116**, 103216. https://doi.org/10.1016/j.compgeo.2019.103216.

Shi, J., Wei, J., Ng, C.W.W., Lu, H., Ma, S., Shi, C. and Li, P. (2022), "Effects of construction sequence of double basement excavations on an existing floating pile", *Tunn. Undergr. Sp. Tech.*, **119**. https://doi.org/10.1016/j.tust.2021.104230.

Shirlaw, J.N., Ong, J.C.W;, Rosser, H.B., Tan, C.G., Osborne, N. H. and Heslop, P.E. (2003), "Local settlements and sinkholes due to EPB tunnelling", *Proceedings of the Institution of Civil Engineers - Geotechnical Engineering*, **156**(4), 193-211. https://doi.org/10.1680/geng.2003.156.4.193

Sivakumar, V., Navaneethan, T., Hughes, D. and Gallagher, G. (2009), "An assessment of the earth pressure coefficient in overconsolidated clays", *Géotechnique*, **59**(10), 825-838. https://doi.org/10.1680/geot.8.P.033

Soomro, M.A., Mangnejo, D.A., Bhanbhro, R., Memon, N.A. and Memon, M.A. (2019), "3D finite element analysis of pile responses to adjacent excavation in soft clay: Effects of different excavation depths systems relative to a floating pile", *Tunn. Undergr. Sp. Tech.*, **86**, 138-155. https://doi.org/10.1016/j.tust.2019.01.012

Soomro, M.A., Mangnejo, D.A. and Mangi, N. (2023), "Investigation of crack growth in a brick masonry wall due to twin perpendicular excavations", *Geomech. Eng.*, **34**(3), 251-265. https://doi.org/10.12989/gae.2023.34.3.251..

Soomro, M., Mangi, N., Mangnejo, D.A. and Zhang, Z. (2023), "The responses of battered pile to tunnelling at different depths relative to the pile length", *Geomech. Eng.*, **35**(6), 603-615. https://doi.org/10.12989/gae.2023.35.6.603.

Soomro, M.A., Ng, C.W.W., Liu, K. and Memon, N.A. (2017), "Pile responses to side-by-side twin tunnelling in stiff clay: Effects of different tunnel depths relative to pile", *Comput. Geotech.*, **84**, 101-116. https://doi.org/10.1016/j.compgeo.2016.11.011.

Soomro, M.A., Liu, K., Mangnejo, D.A. and Mangi, N. (2022), "Effects of twin excavations with different construction sequence on a brick masonry wall: 3D finite element approach", *Structures*, **41**, 866-886. https://doi.org/10.1016/j.istruc.2022.05.060.

Soomro, M.A., Mangnejo, D.A., Saand, A. and Hong, Y. (2022), "Responses of a masonry façade to multi-propped deep excavation-induced ground deformations: 3D numerical parametric study", *Eur. J. Environ. Civil Eng.*, **26**(12), 5983-6011. https://doi.org/10.1080/19648189.2021.1926336.

Soomro, M.A., Mangnejo, D.A., Saand, A. and Mangi, N. (2022), "3D numerical analysis of a masonry façade subjected to excavation-induced ground deformation", *Int. J. Geotech. Eng.*, **16**(7), 865-877. https://doi.org/10.1080/19386362.2021.1937853.

Soomro, M.A., Mangnejo, D.A., Saand, A., Mangi, N. and Zardari, M.A. (2022), "Influence of stress relief due to deep excavation on a brick masonry wall: 3D numerical predictions", *Eur. J. Environ. Civil Eng.*, **26**(15), 7621-7644. https://doi.org/10.1080/19648189.2021.2004450.

Soomro, M.A., Kumar, M., Mangi, N., Mangnejo, D.A. and Cui, Z.D. (2022), "Parametric study of twin tunneling effects on piled foundations in stiff clay: 3D finite-element approach", *Int. J. Geomech.*, **22**(6), 04022079.

Soomro, M.A., Saand, A., Mangi, N., Mangnejo, D.A., Karira, H. and Liu, K. (2021), "Numerical modelling of effects of different multipropped excavation depths on adjacent single piles: Comparison between floating and end-bearing pile responses", *Eur. J. Environ. Civil Eng.*, **25**(14), 2592-2622. https://doi.org/10.1080/19648189.2019.1638312.

Xu, J.M., Wang, C.C., Cheng, Z.L., Xu, T., Zhang, D.W. and Li, Z.L. (2024), "Intelligent prediction model of tunnelling-induced building deformation based on genetic programming and its application", *J. Central South Univ.*, 1-15. https://doi.org/10.1007/s11771-024-5656-x.

Xu, J., Yu, Z., Chen, R., Xu, T., Chen, C. and Wang, Z. (2025a), "Evaluation of the shear stiffness and load redistribution of framed structures affected by tunnelling", *Comput. Geotech.*, **177**, 106899. https://doi.org/10.1016/j.compgeo.2024.106899.

Xu, J., Zheng, L., Yu, Z., Li, Y. and Cai, G. (2025b), "Effects of bending stiffness and interface roughness on tunnel-embedded wall interaction", *Tunn. Undergr. Sp. Tech.*, **155**, 106209. https://doi.org/10.1016/j.tust.2024.106209.

Zheng, G., Peng, S.Y., Ng, C.W.W. and Diao, Y. (2012), "Excavation effects on pile behaviour and capacity", *Can. Geotech. J.*, **49**(12), 1347-1356. https://doi.org/10.1139/t2012-095.

GC